Trade-Offs in Thin Film Solar Cells with Layered Chalcostibite Photovoltaic Absorbers

*Adam W. Welch, Lauryn L. Baranowski, Haowei Peng, Hannes Hempel, Rainer Eichberger, Thomas Unold, Stephan Lany, Colin Wolden, and Andriy Zakutayev**

Discovery of novel semiconducting materials is needed for solar energy conversion and other optoelectronic applications. However, emerging low-dimensional solar absorbers often have unconventional crystal structures and unusual combinations of optical absorption and electrical transport properties, which considerably slows down the research and development progress. Here, the effect of stronger absorption and weaker carrier collection of 2D-like absorber materials are studied using a high-throughput combinatorial experimental approach, complemented by advanced characterization and computations. It is found that the photoexcited charge carrier collection in $CuSbSe_2$ solar cells is enhanced by drift in an electric field, addressing a different absorption/collection balance. The resulting drift solar cells efficiency is <5% due to inherent J_{SC}/V_{OC} trade-off, suggesting that improved carrier diffusion and better contacts are needed to further increase the $CuSbSe_2$ performance. This study also illustrates the advantages of high-throughput experimental methods for fast optimization of the optoelectronic devices based on emerging low-dimensional semiconductor materials.

1. Introduction

Low-dimensional materials have recently attracted scientific attention due to their unusual physical properties[1] and potentially useful applications.[2] In particular, benign grain boundaries[3] and passive free surfaces[4] of binary chalcogenides such as 1D-like Sb_2Se_3 and 2D-like WSe_2 have been studied for future solar energy conversion technologies. Another interesting class of low-dimensional materials is ternary copper chalcogenides, such as $CuPnQ_2$ (Pn = Sb, Bi; Q = S, Se).[5,6] At first glance, $CuSbQ_2$ is very similar to $CuInQ_2$: with a nearly direct band gap of 1.1–1.5 eV, it offers a comparable theoretical solar energy conversion efficiency limit. However, the $CuSbQ_2$ materials have a layered chalcostibite crystal structure (**Figure 1**a), increasing the density of states (DOS) compared to the chalcopyrite $CuInQ_2$. Higher density of states along with difference in electronic structure causes larger optical extinction coefficient and more effective absorption of photons[5] but may also lead to higher effective masses and less efficient collection of the photogenerated charge carriers.

The differences in photon absorption and charge collection often result in different operation mechanisms of the solar cell devices (Figure 1b).[7] As recently summarized in ref.,[8] charge collection mode depends on the ratio of the spatial extent of electric field w (determined by the doping density) to the absorption length d (determined by material composition and structure) of the absorber. Modern high efficiency solar cells have small w/d and operate mainly by diffusion of the photogenerated carriers to selective contacts (Figure 1b), which requires defect-free (e.g., Si[9] and GaAs[10]) and high doping levels. In the alternative case of drift-based operation (e.g., CdTe[11] and hybrid perovskites[12]), the w/d is large so the photogenerated charge carriers are swept to the contacts by a built-in internal electric field that extends throughout the absorber due to low doping, reducing parasitic nonradiative recombination at defect sites. Hence drift operation is typical for materials with stronger optical absorption but weaker carrier collection, like the layered $CuSbSe_2$ discussed here. Of course, in reality this classification is not binary but continuous, with some defect-tolerant absorbers (e.g., $Cu(In,Ga)Se_2$[13] and Cu_3N[14]) showing intermediate w/d ratios and both drift and diffusion charge collection mechanisms.

The materials properties and device performance of the $CuSbSe_2$ absorbers are studied here using high-throughput experimental (HTE) approach (Figure 1c).[15] In this HTE approach, intentional and well-controlled gradients in synthesis conditions are created across the substrate by combinatorial deposition, and the resulting combinatorial sample library is mapped by spatially resolved characterization. In this study, combinatorial libraries of both $CuSbSe_2$ materials and $CuSbSe_2$-based photovoltaic devices are fabricated, allowing for correlation between the performance of solar cells and the physical properties of the absorbers. In addition to these HTE methods, the defect physics is studied by first-principle theoretical calculations, and photoexcited charge carrier dynamics are investigated using transient terahertz (THz) spectroscopy

A. W. Welch, L. L. Baranowski, H. Peng, S. Lany, Dr. A. Zakutayev
National Renewable Energy Laboratory
Golden, CO 80401, USA
E-mail: andriy.zakutayev@nrel.gov
A. W. Welch, L. L. Baranowski, C. Wolden
Colorado School of Mines
Golden, CO 80401, USA
H. Hempel, R. Eichberger, T. Unold
Helmholtz-Zentrum Berlin
14109 Berlin, Germany

DOI: 10.1002/aenm.201601935

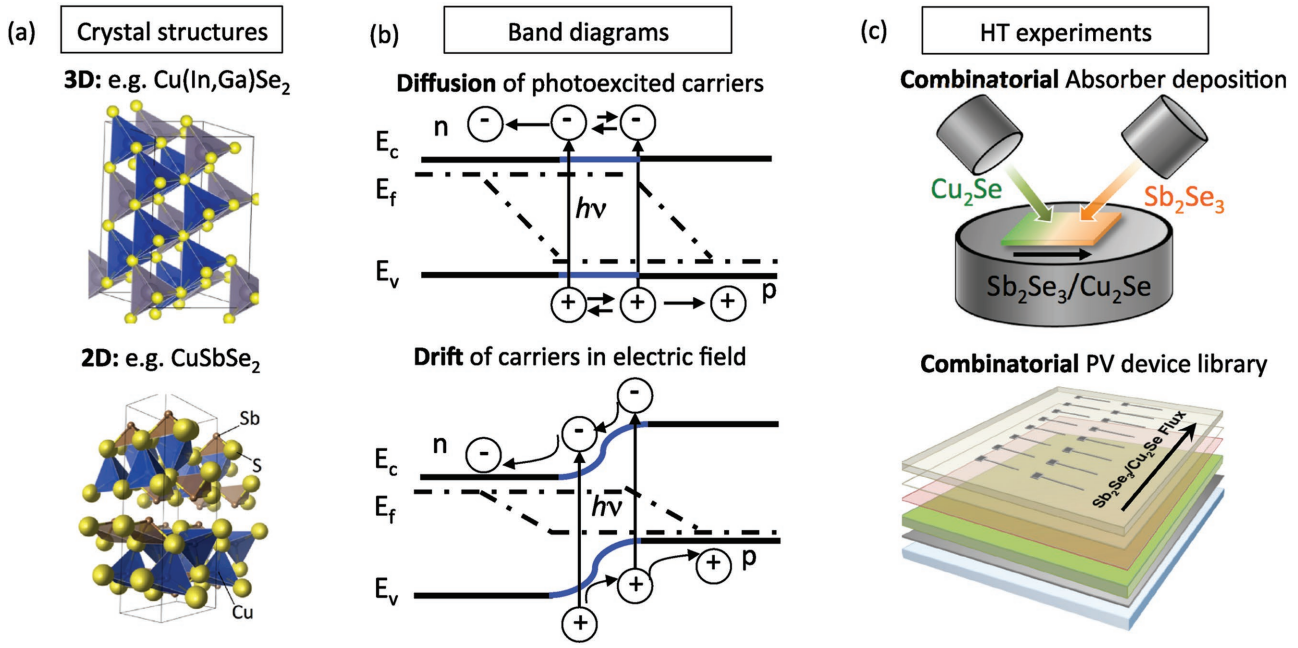

Figure 1. High-throughput experimental studies of drift-dominated solar cells with 2D-like layered absorbers: a) Layered 2D-like chalcostibite structure of $CuSbSe_2$, shown in comparison with the 3D-like structure of $Cu(In,Ga)Se_2$. b) Band diagrams for two types of solar cells at operating conditions, showing diffusion and drift as the two major mechanisms for the photoexcited charge carrier collection. c) Schematics of combinatorial synthesis experiment and the resulting combinatorial PV device library, showing angled guns for the deposition and a grid of top contacts for PV efficiency measurements.

measurements. More details about experimental and theoretical methods used in this paper are provided in the Experimental Section and in the Supporting Information.

2. Results and Discussion

2.1. Materials Synthesis

First, we established deposition conditions that lead to stoichiometric $CuSbSe_2$ material. This can be difficult, since in contrast to $Cu(In,Ga)Se_2$ (CIGS), $Cu_2ZnSn(S,Se)_4$ (CZTS), and Cu_2SnS_3 (CTS) absorber materials, $CuSbSe_2$ is a line compound that exists in the very narrow range of chemical compositions. Here, the exact $CuSbSe_2$ chemical composition was achieved using the "self-regulated" growth process[16] at substrate temperatures above the sublimation point of the Sb_2Se_3 secondary phase[17] (see Figure S1, Supporting Information, for more process details). As shown in **Figure 2**a, the samples deposited at the optimal temperature of 380 °C have a narrow distribution of stoichiometries close to a single $CuSbSe_2$ value of Cu/(Cu + Sb + Se) = 0.25, for a wide range of incoming Sb_2Se_3 fluxes.

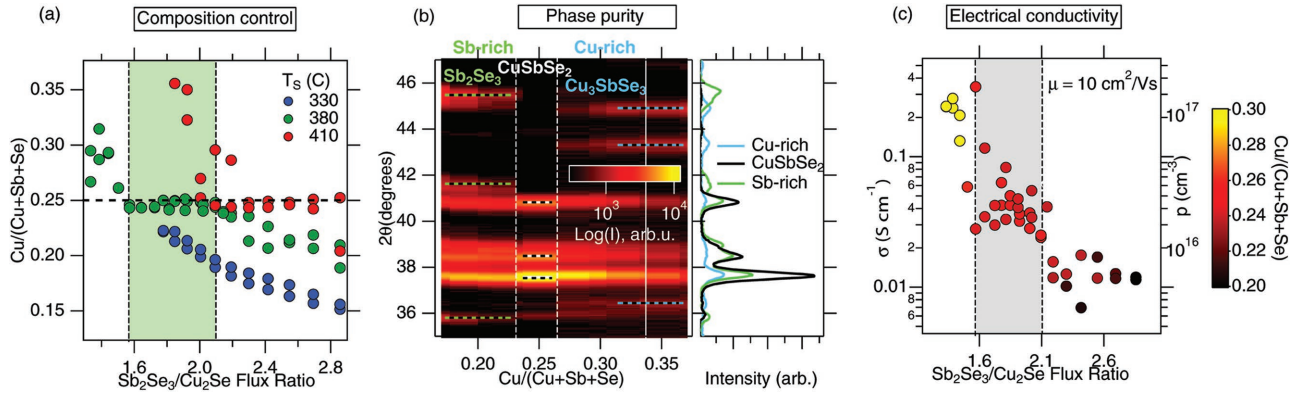

Figure 2. Combinatorial studies of $CuSbSe_2$ absorber material properties: a) Composition control by Sb_2Se_3 overflux for combinatorial libraries grown at substrate temperatures above $CuSbSe_2$ decomposition (red) and below the Sb_2Se_3 sublimation (blue), in comparison with the optimal temperature and flux range (green). b) XRD patterns for the optimal temperature displayed on the color scale as a function of the material stoichiometry, showing evidence of Sb_2Se_3 and Cu_3SbSe_3 impurities off stoichiometry. c) Electrical conductivity, showing intermediate conductivity at Sb_2Se_3 sputter flux ratios that correspond to stoichiometric $CuSbSe_2$ composition (red points).

On the other hand, the samples grown at 330 °C (below Sb_2Se_3 sublimation) and at 410 °C (close to $CuSbSe_2$ decomposition) show a broad range of compositions due to Sb_2Se_3 and Cu_3SbSe_3 precipitates (see Figure S2a, Supporting Information, for the histogram). Thus, the "self-regulated" growth process in excess Sb_2Se_3 vapor at 380 °C allows for facile deposition of the $CuSbSe_2$ films with the desired stoichiometric composition and no phase impurities. In the 380–410 °C temperature range, depending on the incoming Sb_2Se_3/Cu_2Se flux ratio, $CuSbSe_2$ may decompose into Cu_3SbSe_3 solid and Sb_2Se_3 gas.

Next, we present the phase purity of the samples as a function of their precursor flux ratios and resulting chemical composition. Figure 2b shows that most of the measured X-ray diffraction (XRD) patterns fall at the Cu/(Cu + Sb + Se) = 0.25 composition and correspond to $CuSbSe_2$ reference pattern (see Figure S3, Supporting Information, for full range of measured angles). Minor (≈1%) deviations from the $CuSbSe_2$ stoichiometry toward Cu-rich and Sb-rich composition lead to precipitation of Cu_3SbSe_3 and Sb_2Se_3 impurity phases, respectively. To identify the range of processing conditions at which stoichiometric phase-pure $CuSbSe_2$ can be obtained, Raman spectra were studied as a function of incoming Sb_2Se_3/Cu_2Se precursor flux ratio (see Figure S2b, Supporting Information). Vibrational signature of $CuSbSe_2$ phase (strong peak at 210 cm^{-1}) was observed at $1.6 < Sb_2Se_3/Cu_2Se < 2.1$ similar to reports in literature,[18] whereas Cu-rich (195 cm^{-1} peak) and Sb-rich (200 cm^{-1} shoulder) impurities were observed at lower and higher flux ratios, respectively. Since phase-pure stoichiometric $CuSbSe_2$ can be grown in a range of Sb_2Se_3 flux ratios, the flux control may influence other materials properties, such as electrical doping discussed next.

2.2. Electrical Properties

The change in the Sb_2Se_3/Cu_2Se flux ratio (1.6–2.1) without major variation in the resulting $CuSbSe_2$ chemical composition (Figure 2a) corresponds to a subtle gradient in chemical potential that should influence $CuSbSe_2$ point defect chemistry. Since Sb_2Se_3 is kept in the vapor phase, control of its flux is similar to control of oxygen partial pressure (pO_2) during the synthesis of oxides, which has been shown to influence doping.[19] Indeed, conductivity of stoichiometric $CuSbSe_2$ synthesized at 380 °C changes between 0.01 and 0.2 S cm^{-1} (Figure S2c, Supporting Information), limited by the formation of the Sb_2Se_3 and Cu_3SbSe_3 impurities. This range corresponds to a hole concentration of 10^{16}–10^{17} cm^{-3} for the ≈10 cm^2 V^{-1} s^{-1} hole mobility determined from the THz spectroscopy measurements. Zooming into the $CuSbSe_2$ composition (Figure 2c), the conductivity changes with the Sb_2Se_3/Cu_2Se flux ratio, which can be attributed to the increase in the Sb chemical potential. Thus, the Sb_2Se_3/Cu_2Se flux ratio influences the $CuSbSe_2$ defect density and carrier concentration, which is important to many aspects of photovoltaic (PV) device engineering.

To obtain a deeper understanding of the results of the conductivity measurements, we calculated from first principles $CuSbSe_2$ native point defect concentration for different chemical potentials. As shown in **Figure 3**a, the two lowest-energy defects in $CuSbSe_2$ are acceptor-like copper vacancy (V_{Cu}) and donor-like copper interstitials (Cu_i), in agreement with the previously published studies,[20] and in contrast to Cu(In,Ga)Se_2[21] and $Cu_2ZnSn(S,Se)_4$.[22] The resulting hole concentration (Figure 3b) ranges from 10^{16} to 10^{18} cm^{-3} for the 400 °C growth temperature, depending on the chemical potential (see Figure S4, Supporting Information), tightly covering the experimental measurements (Figure 2c). The theoretical calculations also predict deep selenium vacancies (V_{Se}) defects, with relatively high formation enthalpies (1.0–1.5 eV) but amphoteric character (both donor and acceptor states in the gap), which may lead to photoexcited charge carrier trapping. Thus, the extent of electric field in the $CuSbSe_2$ PV device would be determined by shallow V_{Cu} and Cu_i defects, whereas the photoexcited charge carrier lifetime would be influenced by deep V_{Se} defects.

To understand the effects of point defects on photoexcited charge carriers, several selected $CuSbSe_2$ samples were analyzed by transient optical pump THz probe (OPTP) reflection spectroscopy (Figure 3c). The photoexcited charge carrier

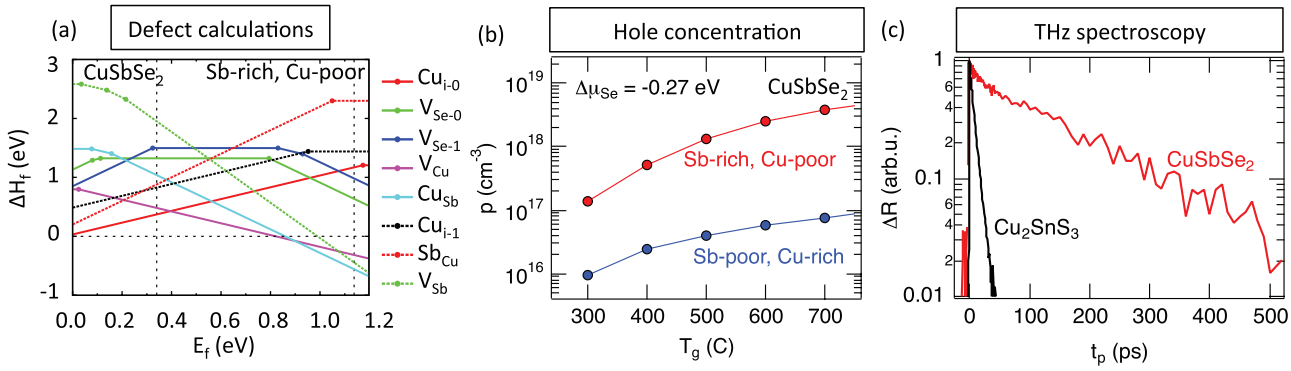

Figure 3. Theoretical and spectroscopic studies of $CuSbSe_2$ properties: a) Theoretical defect formation energies as a function of Fermi level in the $CuSbSe_2$ material for specific conditions (e.g., Sb-rich and Cu-poor). It shows that V_{Cu} and Cu_i are the two dominant doping defects, and V_{Se} is the most significant deep trap defect. b) The calculated room temperature hole concentrations as a function of substrate temperature during film growth, for a constant Se chemical potential of –0.27 eV. c) $CuSbSe_2$ transient THz spectroscopy at 805 nm reveals an electron lifetime of 190 ps, with a small trap state signal at 12 ps, much longer than 7 ps for the annealed Cu_2SnS_3,[26] and a hole mobility of ≈12 cm^2 V^{-1} s^{-1} (not shown).

lifetime determined from these measurements is 0.2 ns, with a small initial 12 ps decay due to trap states, regardless of the flux synthesis condition (Figure S5a, Supporting Information). This $CuSbSe_2$ sample result is similar to that for $CuSbS_2$ samples (0.5–0.7 ns)[23] and is much longer in comparison with the <0.01 ns lifetime measured for Cu_2SnS_3 samples.[24] This Cu_2SnS_3 was chosen for comparison here because it was synthesized in the same chamber under similar conditions as $CuSbS_2$ and $CuSbSe_2$.[25] Given the similar synthesis conditions, this comparison suggests that longer photoexcited carrier lifetime can be achieved in materials with 2D-like layered crystal structure with some point defects (e.g., V_Q in $CuSbQ_2$), compared to 3D-bonded materials with abundant cation disorder (e.g., composition fluctuations in CTS[26,27] and Cu_2ZnSnS_4 (CZTS)[28,29]). However, much more detailed studies would be needed to further support or rule out this hypothesis.

In addition to longer carrier lifetimes (Figure 3c), the frequency-dependent THz spectra (Figure S5b, Supporting Information) indicate favorable transport properties of photoexcited charge carriers in $CuSbSe_2$, in contrast to strong charge localization in cation-disordered Cu_2SnS_3.[26] The DC carrier mobility extracted from these measurements is ≈12 $cm^2\ V^{-1}\ s^{-1}$ and is characteristic of both holes and electrons. The resulting diffusion length ($L_d = (kT\mu\tau/e)^{1/2}$) is estimated to be L_d = 80 nm at room temperature, much shorter compared to CIGS (L_d = 8 µm),[30] which is undesirable for PV device operation. This ≈100× shorter diffusion lengths can be attributed to both shorter lifetimes (τ) due to more defective material and lower mobility (μ) due to ≈10× larger spatially averaged DOS electron effective masses in $CuSbSe_2$ ($m_e^* = 2.5m_0$) compared to $CuInSe_2$ ($m_e^* = 0.26m_0$).[31] Note that the average DOS m_e^* reported here is larger than the anisotropic effective mass in ref. [6]. However, the larger effective mass in $CuSbSe_2$ compared to $CuInSe_2$ also leads to larger absorption coefficient due to higher joint density of states, which may be beneficial for the PV device performance. Given the moderate hole density (Figures 2c and 3b), we expect this different absorption/transport balance in $CuSbSe_2$ to result in drift-enhanced solar cell operation, as opposed to diffusion-dominated photoexcited charge carrier collection typical for CIGS (Figure 1b)

2.3. Photovoltaic Devices

To study the effect of the built-in electric field on the photoexcited charge carrier collection, we fabricated PV devices with $CuSbSe_2$ absorbers grown with varying Sb_2Se_3/Cu_2Se flux ratio (1.4–2.7), thus having different chemical composition (Figure 2a) and different hole concentrations (see Figure 2c). The different hole concentration is expected to cause different spatial extents of build-in electric field of the junction (so-called depletion width). Short circuit current (J_{SC}) and open circuit voltage (V_{OC}) are extracted from the resulting current–voltage (JV) curves measured under illumination (Figure S6a, Supporting Information), and the results are shown in **Figure 4**a as a function of the absorber composition. The V_{OC} remains approximately constant (0.35 eV) in the Cu-poor composition range but falls to zero at the Cu-rich compositions. This demonstrates that the more insulating Sb_2Se_3 impurities, if present in the $CuSbSe_2$, are not as deleterious to the PV device performance as the more conductive Cu_3SbSe_3 impurities. Interestingly, a similar trend is observed for the photocurrent J_{SC}, but with a spike at the Cu/(Cu + Sb + Se) = 0.25 stoichiometric composition, calling for a more detailed investigation of the phase pure $CuSbSe_2$ PV devices.

To elucidate the origin of the variation in J_{SC}, we measured the external quantum efficiency (EQE) spectra as a function of Sb_2Se_3/Cu_2Se flux ratio for the PV devices with phase-pure stoichiometric $CuSbSe_2$ absorbers (Figure 4b). Overall, the relatively low measured EQE (40%–60%) is consistent with the short lifetimes determined from the $CuSbSe_2$ transient THz measurement results (Figure 3c) and may be indicative of interface recombination due to poor band alignment with CdS contact.[25,32] However, a significant increase in EQE is observed with the increasing Sb_2Se_3/Cu_2Se flux ratio, most likely due to better collection of the charge carriers excited by red photons (600–800 nm) in bulk of the absorber (Figure S6b, Supporting Information). This appears to be the dominant effect in the increase of J_{SC} at the stoichiometric $CuSbSe_2$ composition (Figure 4a). Furthermore, according to capacitance–voltage (CV) measurements (Figure S6c, Supporting Information), the depletion width (W) increases and the hole concentration

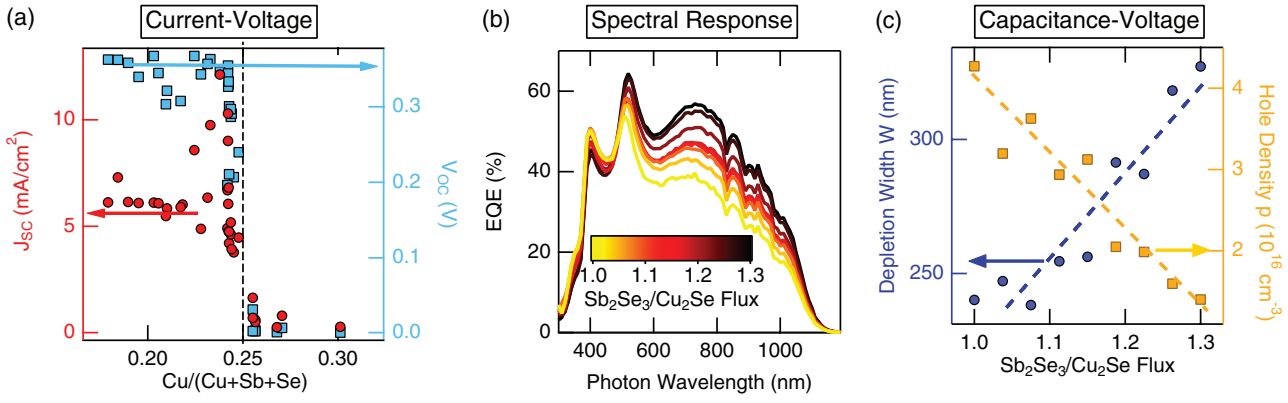

Figure 4. $CuSbSe_2$ PV device performance: a) $CuSbSe_2$ J_{SC} (red) and V_{OC} (blue) as a function of stoichiometry, showing a drop in Cu-rich composition range and a spike in J_{SC} close to stoichiometric composition indicated by vertical dashed line. b) EQE spectra from stoichiometric devices show an increase in red photon (≈750 nm) collection with increasing Sb_2Se_3 overflux, correlating with increase in J_{SC}. c) The results of the CV measurements showing that depletion width (W) increases and hole concentration (p) decreases with increasing Sb_2Se_3/Cu_2Se flux ratio.

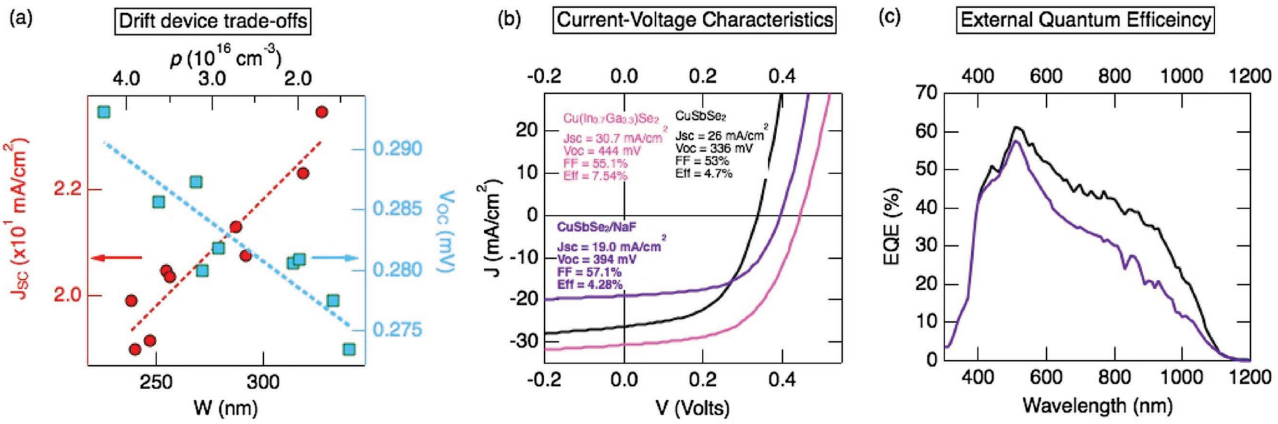

Figure 5. Trade-offs in drift-dominated $CuSbSe_2$ PV devices: a) More photogenerated electrons are collected for larger depletion widths leading to larger J_{SC}, but at the same time V_{OC} is reduced due to decreasing hole concentration. b) The 4.7% efficiency has been achieved by optimizing the V_{OC}/J_{SC} trade-off. Deposition onto an NaF precursor layer leads to better V_{OC} but worse J_{SC} and hence similar efficiency. Both $CuSbSe_2$ efficiencies are lower than the 7.5% efficiency measured for $Cu(In,Ga)Se_2$ with a similar band gap, doping density, and prepared under similar conditions. c) External quantum efficiencies of two $CuSbSe_2$ PV devices, with and without NaF precursor.

(p) decreases with increasing Sb_2Se_3 flux, as shown in Figure 4c. Thus, it can be concluded that the increased EQE (Figure 4b) and J_{SC} (Figure 4a) in $CuSbSe_2$ PV devices can be attributed to enhanced drift collection by built-in electric field with increasing Sb_2Se_3 flux. The alternative explanation of increased minority carrier diffusion length can be ruled out by the flux-independent transient THz spectroscopy measurement results (Figure S5a, Supporting Information).

2.4. Discussion of Trade-Offs

Unfortunately, along with the enhanced J_{SC} (due to larger depletion widths) in a drift PV device comes a suppressed V_{OC} due to decreased carrier concentration: as Fermi level moves toward midgap, the quasi Fermi level splitting (and hence V_{OC}) decreases (Figure 1b). Indeed, the $CuSbSe_2$ PV devices with 0.5 cm^2 total area show both an increase in J_{SC} and a decrease in V_{OC}, with increasing depletion width and decreasing hole concentration determined from CV measurements (**Figure 5**a). After optimizing this trade-off and making other small changes to the device (see Figure S7, Supporting Information, for more details), we were able to achieve J_{SC} of 26 mA cm^{-2} and V_{OC} of 336 mV, which together with a fill factor of 53% resulted in the 4.7% energy conversion efficiency (Figure 5b), with EQE in the 40%–60% range (Figure 5c), for the device of 0.2 cm^2 total area. This is significantly higher efficiency than the previously reported photovoltaic[19,22] and photoelectrochemical[20,33] devices based on $CuSbSe_2$ (1%–2%), and for the structurally related[6,34] but more widely studied[35,36] $CuSbS_2$ absorber material (1%–3%).[37–39] However, the <5% $CuSbSe_2$ drift device efficiency is still lower than the >20% efficiency of, e.g., CdTe drift-based PV devices, most likely due to shorter carrier lifetimes and higher defect densities.

In an effort to break out of the V_{OC}/J_{SC} trade-off, we investigated Na incorporation in the $CuSbSe_2$ absorber by depositing it on a thin 20 nm NaF precursor layer. The $CuSbSe_2$ is deposited at temperatures much lower than CIGS, so it is likely to receive much less Na incorporation from the soda lime glass substrate, known to improve the CIGS PV device performance.[40,41] We found that the Na incorporation enhanced the V_{OC} of $CuSbSe_2$ device by about 50 mV, but again at the expense of J_{SC} (Figure 5b) and EQE (Figure 5c). This clear trade-off in the $CuSbSe_2$ PV device operation contrasts with the performance of CIGS PV devices with a similar band gap and doping density and deposited in the same chamber under similar conditions. As shown in Figure 5b, the CIGS devices have both higher V_{OC} and higher J_{SC}, pointing to photoexcited charge carrier collection by diffusion rather than drift. However, the resulting relatively low 7.5% CIGS efficiency suggests that further optimization of absorber synthesis, such as growth in Se-rich atmosphere, is needed to further increase the $CuSbSe_2$ J_{SC} to the levels comparable with other thin film chalcogenide PV technologies. In addition, as mentioned above,[25,34] contact layers alternative to CdS would be needed to reduce the conduction band offset and increase V_{OC} of the $CuSbSe_2$-based PV devices.

3. Conclusions

We have studied a novel $CuSbSe_2$ absorber using a high-throughput experimental approach combined with first-principles calculations and advanced spectroscopy methods. This study was motivated by the differences in photon absorption and carrier collection between layered semiconductors and tetrahedrally bonded absorber materials. The results of this study show that increasing efficiency of thin film PV solar cells with 2D-like layered absorbers (e.g., $CuSbSe_2$) would require PV device architectures that make use of the different balance between the optical absorption (stronger) and carrier transport (weaker) as compared to 3D-like tetrahedrally bonded materials (e.g., CIGS). The short-term solution presented in this paper is a solar cell with drift-enhanced collection of the photoexcited charge carriers by the electric field. However, the drift-based

solar cells suffer from the trade-off between short circuit current and open circuit voltage, resulting in the $CuSbSe_2$ device efficiency to <5%, which is lower compared to the diffusion-based solar cells with CIGS absorbers prepared under similar conditions. To make successful diffusion-based $CuSbSe_2$ PV devices in long term, more research and development toward higher quality absorbers would be needed, which can be guided by the results of the $CuSbSe_2$ first-principle defect calculations reported here. In addition, an alternative contact material instead of CdS would be needed to reduce interface recombination suggested by overall low EQE. Another conclusion from this study is that high-throughput experiments can quickly reveal the limiting factors of emerging PV absorbers, and that these methods should be used for other semiconductor technologies.

4. Experimental Section

HTE approach was utilized here to study the $CuSbSe_2$ absorbers. Combinatorial cosputtering from binary Cu_2Se and Sb_2Se_3 targets was used to create gradients in chemical composition across the absorber on glass substrates, referred to as a combinatorial sample library (Figure 1c).[42] The depositions also resulted in a region of phase pure stoichiometric $CuSbSe_2$ material with a gradient of chemical potential across the substrate controlled by the Sb_2Se_3 vapor overflux. A similar approach was applied to $CuSbSe_2$ absorbers in the combinatorial PV device libraries (Figure 1c), with Mo back electrode, CdS heterojunction partner at i-ZnO/Al:ZnO front electrode, and Ni/Al contact pad (similar to CIGS).[19,39] More details of the $CuSbQ_2$ (Q = S, Se)[18,19] and Cu_2SnS_3[26,27] thin film deposition and PV device fabrication were published before, and are available in the Supporting Information.

The resulting $CuSbSe_2$ thin films were then measured for chemical composition by X-ray fluorescence (XRF), for phase purity by X-ray diffraction (XRD) and Raman spectroscopy, and for electrical conductivity by custom four-point-probe setup, along 4 rows of 11 points each (44 total points).[43] Selected areas of phase pure material were cleaved from the sample library and characterized by OPTP time-domain and frequency-domain spectroscopy.[44] The frequency dependence in the THz regime extrapolated to this DC-value yields the mobility of electrons and holes, and the scan of the pump–probe delay yields the transient photoinduced conductivity with a resolution of ≈100 fs. The efficiency of all the $CuSbSe_2$ combinatorial PV device libraries was mapped using spatially resolved JV measurements under simulated AM1.5 illumination. For the manual EQE and CV analysis, a separate $CuSbSe_2$ combinatorial device library was grown with a slightly lower deposition temperature and lower Sb_2Se_3/Cu_2Se flux ratios (1.0–1.3), still above the sublimation temperature of Sb_2Se_3. The first-principles calculations were performed with the projected augmented wave method[45] as implemented in the Vienna ab initio simulation package.[46] The defect properties were investigated via the standard supercell method[47] with appropriate corrections.[48] More details about the first principle calculations and various experimental characterization methods can be found in the Supporting Information.

Supporting Information

Supporting Information is available from the Wiley Online Library or from the author.

Acknowledgements

The work was supported by the U. S. Department of Energy, Office of Energy Efficiency and Renewable Energy, as a part of the SunShot initiative, under Contract No. DE-AC36-08GO28308 to National Renewable Energy Laboratory. The authors would like to thank Clay DeHart and Carolyn Beall for technical assistance as well as Eric Toberer and F. Willian de S. Lucas for useful discussions.

Received: September 1, 2016
Revised: November 15, 2016
Published online:

[1] K. F. Mak, C. Lee, J. Hone, J. Shan, T. F. Heinz, *Phys. Rev. Lett.* **2010**, *105*, 136805.
[2] A. Pospischil, M. M. Furchi, T. Mueller, *Nat. Nanotechnol.* **2014**, *9*, 257.
[3] Y. Zhou, L. Wang, S. Chen, S. Qin, X. Liu, J. Chen, D. J. Xue, M. Luo, Y. Cao, Y. Cheng, E. H Sargent, *Nat. Photonics* **2015**, *9*, 409.
[4] Y. Liu, P. Stradins, S. H. Wei, *Sci. Adv.* **2016**, *2*, e1600069.
[5] L. Yu, R. S. Kokenyesi, D. A. Keszler, A Zunger, *Adv. Energy Mater.* **2013**, *3*, 43.
[6] D. J. Temple, A. B. Kehoe, J. P. Allen, G. W. Watson, D. O. Scanlon, *J. Phys. Chem. C* **2012**, *1167*334.
[7] U. Rau, D. Abou-Ras, T. Kirchartz, *Advanced Characterization Techniques for Thin Film Solar Cells*, John Wiley & Sons, Weinheim, Germany, **2011**.
[8] T. Kirchartz, J. Bisquert, I. Mora-Sero, G. Garcia-Belmonte, *Phys. Chem. Chem. Phys.* **2015**, *17*, 4007.
[9] J. Bullock, M. Hettick, J. Geissbühler, A. J. Ong, T. Allen, C. M. Sutter-Fella, T. Chen, H. Ota, E. W. Schaler, S. De Wolf, C. Ballif, *Nat. Energy* **2016**, *1*, 15031.
[10] E. D. Kosten, J. H. Atwater, J. Parsons, A. Polman, H. A. Atwater, *Light: Sci. Appl.* **2013**, *2*, e45.
[11] J. M. Burst, J. N. Duenow, D. S. Albin, E. Colegrove, M. O. Reese, J. A. Aguiar, C. S. Jiang, M. K. Patel, M. M. Al-Jassim, D. Kuciauskas, S. Swain, *Nat. Energy* **2016**, *1*, 16015.
[12] R. E. Brandt, V. Stevanović, D. S. Ginley, T. Buonassisi, *MRS Commun.* **2015**, *5*, 265.
[13] A. Chirilă, S. Buecheler, F. Pianezzi, P. Bloesch, C. Gretener, A. R. Uhl, C. Fella, L. Kranz, J. Perrenoud, S. Seyrling, R. Verma, *Nat. Mater.* **2011**, *10*, 857.
[14] A. Zakutayev, C. M. Caskey, A. N. Fioretti, D. S. Ginley, J. Vidal, V. Stevanovic, E. Tea, S. Lany, *J. Phys. Chem. Lett.* **2014**, *5*, 1117.
[15] M. L. Green, I. Takeuchi, J. R. Hattrick-Simpers, *J. Appl. Phys.* **2013**, *113*, 231101.
[16] A. W. Welch, P. P. Zawadzki, S. Lany, C. A. Wolden, A. Zakutayev, *Sol. Energy Mater. Sol. Cells* **2015**, *132*, 499.
[17] A. W. Welch, L. L. Baranowski, P. Zawadzki, S. Lany, C. A. Wolden, A. Zakutayev, *Appl. Phys. Exp.* **2015**, *8*, 082301.
[18] D. Tang, J. Yang, F. Liu, Y. Lai, M. Jia, J. Li, Y. Liu, *Electrochem. Solid-State Lett.* **2011**, *15*, D11.
[19] A. Zakutayev, N. H. Perry, T. O. Mason, D. S. Ginley, S. Lany, *Appl. Phys. Lett.* **2013**, *103*, 232106.
[20] D. J. Xue, B. Yang, Z. K. Yuan, G. Wang, X. Liu, Y. Zhou, L. Hu, D. Pan, S. Chen, J. Tang, *Adv. Energy Mater.* **2015**, *5*, 1501203.
[21] S. H. Wei, S. B. Zhang, A. Zunger, *Appl. Phys. Lett.* **1998**, *72*, 3199.
[22] S. Chen, X. G. Gong, A. Walsh, S. H. Wei, *Appl. Phys. Lett.* **2010**, *96*, 021902.
[23] F. W. de Souza Lucas, A. W. Welch, L. L. Baranowski, P. C. Dippo, H. Hempel, T. Unold, R. Eichberger, B. Blank, U. Rau, L. H. Mascaro, A. Zakutayev, *J. Phys. Chem. C* **2016**, *120*, 18377.
[24] L. L. Baranowski, K. McLaughlin, P. Zawadzki, S. Lany, A. Norman, H. Hempel, R. Eichberger, T. Unold, E. S. Toberer, A. Zakutayev, *Phys. Rev. Appl.* **2015**, *4*, 044017.
[25] L. L. Baranowski, P. Zawadzki, S. Christensen, D. Nordlund, S. Lany, A. C. Tamboli, L. Gedvilas, D. S. Ginley, W. Tumas, E. S. Toberer, A. Zakutayev, *Chem. Mater.* **2014**, *26*, 4951.

[26] P. Zawadzki, A. Zakutayev, S. Lany, *Phys. Rev. Appl.* **2015**, *3*, 034007.
[27] P. Zawadzki, A. Zakutayev, S. Lany, *Phys. Rev. B* **2015**, *92*, 201204.
[28] J. J. Scragg, L. Choubrac, A. Lafond, T. Ericson, C. Platzer-Björkman, *Appl. Phys. Lett.* **2014**, *104*, 041911.
[29] T. Gokmen, O. Gunawan, D. B. Mitzi, *Appl. Phys. Lett.* **2014**, *105*, 033903.
[30] J. V. Li, S. Grover, M. A. Contreras, K. Ramanathan, D. Kuciauskas, R. Noufi, *Sol. Energy Mater. Sol. Cells* **2014**, *124*, 143.
[31] Effective masses and other electronic struture parameters are available at www.materials.nrel.gov, accessed: December, **2016**.
[32] S. Siol, P. Schultz, M. Young, K. A. Borup, G. Teeter, A. Zakutayev, *Adv. Mater. Interfaces*, **2016**, *3*, 1600755.
[33] D. Colombara, L. M. Peter, K. D. Rogers, J. D. Painter, S. Roncallo, *Thin Solid Films* **2011**, *519*, 7438.
[34] J. T. Dufton, A. Walsh, P. M. Panchmatia, L. M. Peter, D. Colombara, M. S. Islam, *Phys. Chem. Chem. Phys.* **2012**, *14*, 7229.
[35] R. E. Ornelas-Acosta, D. Avellaneda, S. Shaji, G. A. Castillo, T. D. Roy, B Krishnan, *J. Mater. Sci.: Mater. Electron.* **2014**, *25*, 4356.
[36] Y. Rodrıguez-Lazcano, M. T. S. Nair, P. K. Nair, *J. Cryst. Growth* **2001**, *223*, 399.
[37] A. W. Welch, L. L. Baranowski, P. Zawadzki, C. DeHart, S. Johnston, S. Lany, C. A. Wolden, A. Zakutayev, *Prog. Photovoltaics* **2016**, *24*, 929.
[38] W. Septina, S. Ikeda, Y. Iga, T. Harada, M. Matsumura, *Thin Solid Films* **2014**, *550*, 700.
[39] B. Yang, L. Wang, J. Han, Y. Zhou, H. Song, S. Chen, J. Zhong, L. Lv, D. Niu, J. Tang, *Chem. Mater.* **2014**, *26*, 3135.
[40] L. Kronik, D. Cahen, H. W. Schock, *Adv. Mater.* **1998**, *10*, 31.
[41] S. H. Wei, S. B. Zhang, A. Zunger, *J. Appl. Phys.* **1999**, *85*, 7214.
[42] A. N. Fioretti, A. Zakutayev, H. Moutinho, C. Melamed, J. D. Perkins, A. G. Norman, M. Al-Jassim, E. S. Toberer, A. C. Tamboli, *J. Mater. Chem. C* **2015**, *3*, 11017.
[43] A. Zakutayev, F. J. LucianoIV, V. P. Bollinger, A. K. Sigdel, P. F. Ndione, J. D. Perkins, J. J. Berry, P. A. Parilla, D. S. Ginley, *Rev. Sci. Instrum.* **2013**, *84*, 053905.
[44] T. Unold, H. Hempel, C. Strothkämper, C. A. Kaufmann, R. Eichberger, A. Bartelt, *2014 IEEE 40th Photovoltaic Spec. Conf. (PVSC)*, **2014**, p. 2066, IEEE, Piscataway, NJ, USA.
[45] P. E. Blöchl, *Phys. Rev. B* **1994**, *50*, 17953.
[46] G. Kresse, J. Furthmüller, *Phys. Rev. B* **1996**, *54*, 11169.
[47] S. Lany, A. Zunger, *Phys. Rev. B* **2008**, *78*, 235104.
[48] H. Peng, D. O. Scanlon, V. Stevanovic, J. Vidal, G. W. Watson, S. Lany, *Phys. Rev. B* **2013**, *88*, 115201.